



Systemic siRNA Delivery to Tumors by Cell-Penetrating α -Helical Polypeptide-Based Metastable Nanoparticles

Journal:	<i>Nanoscale</i>
Manuscript ID	NR-ART-05-2018-003976.R1
Article Type:	Paper
Date Submitted by the Author:	19-Jun-2018
Complete List of Authors:	<p>Liu, Yang; University of Illinois at Urbana-Champaign, Materials Science and Engineering Song, Ziyuan; University of Illinois at Urbana-Champaign, Materials Science and Engineering Zheng, Nan; University of Illinois at Urbana-Champaign, Materials Science and Engineering Nagasaka, Kenya; University of Illinois at Urbana-Champaign Yin, Lichen; Soochow University, Institute of Functional Nano & Soft Materials (FUNSOM) Cheng, Jianjun; University of Illinois at Urbana-Champaign, Materials Science and Engineering</p>

1 **Systemic siRNA Delivery to Tumors by Cell-Penetrating α -Helical**

2 **Polypeptide-Based Metastable Nanoparticles**

3

4 Yang Liu[†], Ziyuan Song[†], Nan Zheng[†], Kenya Nagasaka[‡], Lichen Yin^{⊥,*}, Jianjun Cheng^{†,¶,A,C,•,•,£,⊥,*}

5

6 [†]Department of Materials Science and Engineering, University of Illinois at Urbana-Champaign, Illinois
7 61801, USA, [‡]School of Molecular and Cellular Biology, University of Illinois at Urbana-Champaign,
8 Illinois 61801, USA, [¶]Frederick Seitz Materials Research Laboratory, University of Illinois at Urbana-
9 Champaign, Urbana, IL 61801, USA, ^ADepartment of Bioengineering, University of Illinois at Urbana-
10 Champaign, Urbana, IL 61801, USA, ^CBeckman Institute for Advanced Science and Technology,
11 University of Illinois at Urbana-Champaign, Urbana, IL 61801, USA, [•]Department of Chemistry,
12 University of Illinois at Urbana-Champaign, Urbana, IL 61801, USA, [•]Carl R. Woese Institute for
13 Genomic Biology, University of Illinois at Urbana-Champaign, Urbana, IL 61801, USA, [£]Micro and
14 Nanotechnology Lab, University of Illinois at Urbana-Champaign, Urbana, IL 61801, USA, [⊥]Jiangsu Key
15 Laboratory for Carbon-Based Functional Materials & Devices, Institute of Functional Nano & Soft
16 Materials (FUNSOM), Collaborative Innovation Center of Suzhou Nano Science and Technology, Joint
17 International Research Laboratory of Carbon-Based Functional Materials and Devices, Soochow
18 University, Suzhou 215123, China

19

20 *Corresponding author: jianjunc@illinois.edu (J.C.); leyin@suda.edu.cn (L.Y.)

21

22

1 **Abstract**

2 Systemic, non-viral siRNA delivery for cancer treatment is mainly achieved *via* condensation by
3 cationic materials (e.g., lipids and cationic polymers), which nevertheless, suffers from poor
4 serum stability, non-specific tissue interaction, and unsatisfactory membrane activity against
5 efficient *in vivo* gene knockdown. Here, we report the design of a metastable, cancer-targeting
6 siRNA delivery system based on two functional polymers, PVBLG-8, a cationic, helical cell-
7 penetrating polypeptide, and poly(L-glutamic acid) (PLG), an anionic random-coiled polypeptide.
8 PVBLG-8 with rigid, linear structure showed weak siRNA condensation capability, and PLG
9 with flexible chains was incorporated as a stabilizer which provided sufficient molecular
10 entanglement with PVBLG-8 to encapsulate the siRNA within the polymeric network. The
11 obtained PVBLG-8/siRNA/PLG nanoparticles (PSP NPs) with positive charges were
12 sequentially coated with additional amount of PLG, which reversed the surface charge from
13 positive to negative to yield the metastable PVBLG-8/siRNA/PLG@PLG (PSPP) NPs. The
14 PSPP NPs featured desired serum stability during circulation to enhance tumor accumulation *via*
15 the enhanced permeability and retention (EPR) effect. Upon acidification in the tumor
16 extracellular microenvironment and intracellular endosomes, the partial protonation of PLG on
17 PSPP NPs surface would lead to dissociation of PLG coating from NPs, exposure of the highly
18 membrane-active PVBLG-8, and surface charge reversal from negative to positive, which
19 subsequently promoted tumor penetration, selective cancer cell internalization, and efficient
20 endolysosomal escape. When siRNA against epidermal growth factor receptor (EGFR) was
21 encapsulated, the PSPP NPs showed excellent tumor penetration capability, tumor cell uptake
22 level, EGFR silencing efficiency, and tumor growth inhibition efficacy in U-87 MG glioblastoma
23 tumor spheroids *in vitro* and in xenograft tumor-bearing mice *in vivo*, outperforming the PSP

1 NPs and several commercial reagents such as Lipofectamine 2000 and poly(L-lysine) (PLL). This
2 study therefore demonstrates a facile and unique design approach of metastable and charge
3 reversal NPs, which overcomes multiple biological barriers against systemic siRNA delivery
4 toward anti-cancer treatment.

5

6 **Keywords:** siRNA delivery, α -helical polypeptide, cell penetrating peptide, metastable
7 nanoparticles (NPs), anti-cancer gene therapy

8

1 **Introduction**

2 RNA interference (RNAi) is a post-transcriptional regulation process mainly mediated by small
3 interfering RNA (siRNA), which leads to mRNA degradation in a sequence-specific manner.
4 RNAi has emerged as a promising therapeutic modality for cancer treatment.¹⁻⁹ Compared to
5 chemotherapy with poor therapeutic selectivity and unsatisfactory efficacy,^{10, 11} RNAi provides a
6 more selective and specific treatment paradigm to regulate the abnormal genes in cancer cells.^{12,}
7 ¹³ Most of the current siRNA therapeutics in the clinical trials utilize direct administration into
8 local target sites such as the eye and lung.¹⁴ Due to the difficulty in locating the tumor areas or
9 defining the margins of tumors such as glioma,^{2, 15} it is necessary to develop the systemically
10 delivered siRNA formulation.

11 Cationic polymers, such as chitosan, poly(L-lysine) (PLL), and polyethylenimine (PEI), have
12 been widely applied in siRNA delivery by forming stable, charged nanoparticles (NPs) via
13 electrostatic complexation with siRNA.^{16, 17} While efficient in siRNA complexation, these
14 carriers often lack strong membrane activities toward intracellular siRNA delivery, and
15 endolysosomal entrapment post endocytosis always remains a critical hurdle against polycation-
16 mediated siRNA delivery. Additionally, because siRNA is short and linear nucleic acid,
17 polycations with high cationic charge density are often required to enable efficient complexation
18 with siRNA and to promote the interaction with cell membranes toward potentiated gene
19 silencing efficiency.¹⁸ However, the positive surface charges could also interact with the
20 negatively charged serum proteins during circulation, which provokes capture of NPs by the
21 reticuloendothelial system (RES) tissues (such as liver and spleen) yet low distribution levels in
22 tumors. PEGylation is the most commonly utilized approach to address this issue, which shields
23 the surface positive charges to improve serum stability, prolong blood circulation, and facilitate

1 passive tumor targeting.^{19, 20} Nevertheless, PEGylation at the meantime reduces the binding
2 affinity between NPs and cell membranes, which prevents effective tumor accumulation and cell
3 uptake to hinder the gene knockdown efficiency^{21, 22} Sheddable PEGylation that could be
4 removed in response to tumor-specific triggers serves as an alternative strategy, which however,
5 requires tedious chemical synthesis with difficulty in consistency control. Therefore,
6 development of a serum-stable and cancer-targeting siRNA delivery system capable of potent
7 and selective tumor penetration and membrane permeation is of great interest toward anti-cancer
8 gene therapy.

9 Recently, we developed PVBLG-8, a unique membrane-penetrating, cationic polypeptide, which
10 possesses stable α -helical secondary structure and helix-dependent membrane penetration
11 capability with 1-2 orders of magnitude higher than conventional cationic polypeptides such as
12 PLL or short cell penetrating peptides (CPPs) such as HIV-Tat and Arg9.^{2, 23-28} As a result, it can
13 condense DNA and demonstrates potent DNA transfection efficiencies to outperform
14 commercial transfection reagents such as Lipofectamine 2000. However, it shows poor siRNA
15 complexation capability and only results in a loosely condensed structure, mainly because
16 siRNA is linear and rod-like structure with few anionic charges compared to DNA molecules,
17 which provides insufficient molecular entanglement or electrostatic interaction with PVBLG-8
18 that also adopts linear and rigid rod-like structure.²³

19 To enhance the siRNA encapsulation efficiency of PVBLG-8, we were inspired by the success of
20 PVBLG-8/DNA and other polycations/DNA encapsulation mechanisms, and herein incorporated
21 poly(L-glutamic acid) (PLG), a biodegradable and biocompatible anionic polypeptide already
22 used in multiple clinical trials,²⁹ for the formation of PVBLG-8/siRNA complexes.^{30, 31} Similar
23 to DNA, PLG possesses rich negative charges and flexible backbone to allow efficient

1 complexation with PVBLG-8 via molecular entanglement.³² When PLG and siRNA were co-
2 complexed with PVBLG-8, PLG serves as a physical crosslinker to promote and stabilize the
3 formation of NPs, and in the meantime to facilitate effective encapsulation of siRNA into the
4 polymeric nano-structure. PVBLG-8/siRNA/PLG (PSP) NPs with positively charged surfaces
5 were thus obtained (Scheme 1). Similar to other polycationic siRNA delivery NPs, PSP NPs also
6 suffer from poor serum stability, tumor accumulation, and non-specific membrane penetration.
7 The microenvironment of tumor offers various biomarkers to distinguish it from normal
8 tissues.³³⁻³⁵ In particular, the acidic pH in the extracellular compartment of tumor tissues has
9 attracted great interest for the development of pH-responsive systems toward tumor-specific drug
10 delivery.³⁶⁻⁴⁰ By taking advantage of this unique tumor-specific physiology, NPs could be
11 designed to be non-charged or negatively charged during systemic circulation while transform
12 into positively charged state in response to the acidic pH to enable cancer-specific tumor
13 penetration and cellular internalization.^{19, 41} In support of such strategy, the surface of PSP NPs
14 was further coated with PLG, yielding the metastable PVBLG-8/siRNA/PLG@PLG (PSPP) NPs
15 with negatively charged surfaces which accordingly afforded desired serum stability and
16 enhanced tumor accumulation (Scheme 1). In the acidic extracellular compartment in the tumor
17 tissues, the surface PLG could be partially protonated, thus triggering removal of the PLG
18 coating and exposure of the cationic, membrane-active PVBLG-8 to subsequently potentiate the
19 tumor penetration, cell internalization, and endosomal escape for efficient RNAi. Unlike
20 previously reported charge-reversal strategy using acid-cleavable covalent conjugation with
21 neutral or negative moieties, the metastable PLG coating offered an immediate and quick
22 response to the acidic tumor microenvironment to enable de-shielding.⁴² siRNA against
23 endothelial growth factor receptor (EGFR), a growth factor receptor that induced cell

1 differentiation and proliferation upon activation through the binding of its ligands and
2 overexpressed in many types of tumors,⁴³ was encapsulated by the PSPP NPs. The tunable tumor
3 penetration, cancer-selective cell internalization, EGFR knockdown efficiency, and anti-tumor
4 efficacy were mechanistically explored in U-87 MG glioblastoma tumor spheroids *in vitro* and in
5 xenograft tumor-bearing mice *in vivo*.

6 **Experimental**

7 **Materials, Cells, and Animals**

8 EGFR siRNA duplex and negative control siRNA with scrambled sequences (sc) were purchased
9 from Integrated DNA Technologies (Coralville, Iowa, USA) and were dissolved in DEPC-
10 treated water before use. The siRNA sequences were shown in Table S1. Cy3-labeled EGFR
11 siRNA duplex (Cy3-siRNA) was used for *in vitro* cell uptake studies, while Cy5-labeled EGFR
12 siRNA duplex (Cy5-siRNA) was used for the *in vivo* imaging study. PVBLG-8 was synthesized
13 following previously published procedures.²

14 U-87 MG cells (human glioblastoma) were purchased from the American Type Culture
15 Collection (Rockville, MD, USA), and were cultured in DMEM supplemented with 10% fetal
16 bovine serum (FBS). HEK-293 cells were kindly provided by Prof. Kemper (University of
17 Illinois at Urbana-Champaign) and were cultured in DMEM containing 10% FBS.

18 Athymic nude mice (8-10 week) were obtained from Charles River Laboratory (Wilmington,
19 MA, USA) and were housed in an SPF room with four mice per cage. Mice were given access to
20 water *ad libitum* and exposed to a 12:12 h light-dark cycle (7:00 am-7:00 pm) at 25 ± 1 °C. All
21 animal studies were performed in strict accordance with the NIH guidelines for the care and use
22 of laboratory animals (NIH Publication No. 85-23 Rev. 1985). The animal experimental

1 protocols were approved by the Institutional Animal Care and Use Committees (IACUC) of
2 University of Illinois at Urbana-Champaign.

3

4 **Instrumentation**

5 ¹H NMR spectra were recorded on a Varian U500 (500 MHz) spectrometer. Electrospray
6 ionization mass spectrometry (ESI-MS) was performed on a Waters Quattro-Mass Spectrometer.
7 Matrix Assisted Laser Desorption Ionization-Time Of Flight mass spectrometry (MALDI-TOF-
8 MS) was performed on an Applied Biosystems Voyager-DE STR Time of Flight instrument or a
9 Bruker Daltonics UltrafleXtreme MALDI-TOF instrument in positive-ion mode with 2,5-
10 dihydroxybenzoic acid as a matrix. Gel permeation chromatography (GPC) experiments were
11 performed on a system equipped with an isocratic pump (Model 1100, Agilent Technology,
12 Santa Clara, CA, USA), a DAWN HELEOS multi-angle laser light scattering (MALLS) detector
13 (Wyatt Technology, Santa Barbara, CA, USA), and an Optilab rEX refractive index detector
14 (Wyatt Technology, Santa Barbara, CA, USA). The detection wavelength of HELEOS was set at
15 658 nm. Separations were performed using serially connected size exclusion columns (100 Å,
16 500 Å, 103Å, and 104 Å Phenogel columns, 5 μm, 300 × 7.8 mm, Phenomenex, Torrance, CA,
17 USA) at 60 °C using DMF containing 0.1 M LiBr as the mobile phase. The MALLS detector
18 was calibrated using pure toluene with no need for calibration using polymer standards and can
19 be used for the determination of the absolute molecular weights (MWs). The MWs of polymers
20 were determined based on the dn/dc value of each polymer sample calculated offline using the
21 internal calibration system processed by the ASTRA V software (Version 5.1.7.3,
22 WyattTechnology, CA, USA). Lyophilization was performed on a FreeZone lyophilizer
23 (Labconco, MO, USA).

1

2 **Preparation and Characterization of NPs**

3 PVBLG-8 and PLG were synthesized as previously reported²⁶ with polymerization degrees
4 of 195 and 50, respectively. siRNA, PVBLG-8, and PLG were separately dissolved in
5 DEPC-treated water at 0.2, 1, and 1 mg/mL, respectively. siRNA and PLG were mixed (1:5,
6 w/w), into which PVBLG-8 was added at the PVBLG-8/PLG weight ratio of 10:1. The
7 mixture was vortexed for 30 s and incubated at 37 °C for 30 min to obtain the PSP NPs. The
8 PSP NPs were further coated with PLG via addition of the PLG solution (1 mg/mL in
9 DEPC water) at various PLG/PVBLG-8 weight ratios with gentle shaking, thus achieving
10 the PLG-coated PSP (PPSP) NPs. A gel retardation assay was used to evaluate the siRNA
11 condensation efficiency. Briefly, NPs or naked siRNA were loaded in 4% agarose gel
12 followed by electrophoresis at 56 V for 1 h and visualization of siRNA migration using the
13 gel documentation. The NPs were also subjected to size and zeta potential measurement
14 using dynamic light scattering (DLS, Zetasizer Nano-ZS, Malvern Instruments, UK). To
15 explore the detachment of surface PLG from NPs, the zeta potentials of NPs were
16 monitored at different pH values (7.4, 6.5, and 5.5). To evaluate the stability of NPs in
17 serum, NPs were diluted with DMEM containing 10% FBS for 10 fold and incubated at RT
18 for 2 h before size measurement using DLS.

19

20 **Stability of siRNA in NPs**

21 In order to evaluate the *in vivo* stability of siRNA following systemic administration, siRNA-
22 containing NPs or naked siRNA were incubated with 10% mouse serum at 37 °C for 2 h. The
23 mixture was heated at 80 °C for 5 min to deactivate the nucleases, and heparin (1000 U/mL) was

1 then added to dissociate the siRNA. The mixture was loaded on 4% agarose gel followed by
2 electrophoresis at 56 V for 1 h, and the siRNA integrity was visualized by gel documentation. .

3

4 **Cellular Uptake**

5 U-87 MG cells were seeded on 24-well plates at 5×10^4 cells/well and cultured for 24 h. To
6 mimic the acidic pH in the tumor environment, the medium was replaced by HBSS (pH 6.5), and
7 Cy3-siRNA-containing NPs or naked Cy3-siRNA were added (0.4 μ g siRNA/well, 200 μ L/well)
8 followed by incubation at 37 °C for 4 h. Poly(L-lysine) (PLL, MW = 70-150 kDa)/siRNA NPs
9 (w/w = 20:1) were incorporated as a control. Cells were washed with PBS for three times and
10 then lysed with the RIPA lysis buffer (100 μ L). The Cy3-siRNA level in the lysate was
11 determined by spectrofluorimetry ($\lambda_{\text{ex}}=480$ nm, $\lambda_{\text{em}}=520$ nm), and the total protein content was
12 determined using the BCA kit. The cell uptake level was expressed as the fluorescence intensity
13 of Cy3-siRNA per 1 mg of cellular protein.

14 To explore the endosomal escape of NPs, cells were co-incubated with LysoTracker Green and
15 Cy3-siRNA-containing NP at pH 6.5 for 0.5 h and 2 h at 37 °C, respectively. Cells were then
16 fixed with 4% paraformaldehyde (PFA), nuclei-stained with Hoechst, and observed by CLSM
17 (Confocal laser scanning microscopy) (Model 700, Zeiss, Germany).

18 HEK293 cells were incubated with naked siRNA, PSP NPs and PSPP NPs in HBSS (pH 7.4) for
19 4 h, respectively. Cells were washed with PBS three times and then lysed with the RIPA lysis
20 buffer. The fluorescence intensity of Cy3-siRNA in the lysate was determined by
21 spectrofluorimetry ($\lambda_{\text{ex}}=480$ nm, $\lambda_{\text{em}}=520$ nm); the total protein content was determined by
22 BCA assay. Uptake level was expressed as the fluorescence intensity of Cy3-siRNA per mg of
23 cellular protein.

1

2 *In vitro* penetration in 3D tumor spheroids

3 Low-melting-point agarose was dissolved in sterile PBS (pH 7.4) at the final concentration of
4 1.5%.⁴⁴ The agarose solution was added to 96-well plate (50 μ l/well), and agarose-coated plates
5 were obtained after being fully cooled. The agarose-coated plates were exposed under UV light
6 for 30 min for sterilization. U-87 MG cells were then seeded on the agarose-coated plates at
7 1×10^5 cells/well and cultured for 7 days to allow formation of 3D tumor spheroids. The medium
8 was changed every other day. PPSP NPs prepared from Alexa Fluor-488-labeled PLG and Cy3-
9 siRNA were added (0.4 μ g siRNA/well, 200 μ L/well) and incubated with spheroids in serum-
10 free medium (pH 6.5 or 7.4) for 4 h. Then, the tumor spheroids were washed with PBS for three
11 times and fixed with 4% PFA. Cell nuclei were stained with Hoechst, and the penetration of NPs
12 into tumor spheroids was observed by CLSM (Model 700, Zeiss, Germany).

13

14 *In Vitro* EGFR knockdown in U-87 MG cells

15 U-87 MG cells were seeded on 6-well plates at 5×10^5 cells/well and cultured for 24 h. The
16 medium was changed to serum-free DMEM (pH 6.5), and PPSP NPs were added at pre-
17 determined siRNA concentrations. Following incubation for 4 h, the medium was replaced with
18 serum-containing DMEM, and cells were further cultured for 20 h. The EGFR mRNA level was
19 determined by real-time PCR, and results were represented as the percentage of EGFR mRNA
20 levels of control cells that did not receive NPs treatment. To prepare the samples for real-time
21 PCR analysis, RNA was isolated from cells using the QIAGEN RNeasy Mini Kit. cDNA was
22 synthesized from 5 μ g of total RNA using high capacity cDNA reverse transcription kit (Applied
23 Biosystems, CA, USA) according to the manufacturer's protocol. Synthesized cDNA, EGFR

1 primers (forward and reverse, sequences shown in Table S2), and SYBR Premix Ex Taq™
2 were mixed and run on an ABI PRISM 7900HT Real-Time PCR system (Applied Biosystems,
3 CA, USA). The GAPDH mRNA was used as an internal loading control, and its expression did
4 not change upon addition of NPs or siRNA.

5

6 ***In vitro* anti-tumor efficacy in 3D tumor spheroids**

7 The 3D tumor spheroids were prepared as described above. On day 3 post tumor cell seeding, the
8 spheroids were treated with different NPs in HBSS (pH 6.5 or 7.4) for 4 h. The spheroids were
9 further cultured for 20 h, and the EGFR mRNA levels in the tumor spheroids were determined
10 by real-time PCR. Sizes of the spheroids treated by various NPs at pH 6.5 were observed by
11 optical microscopy on day 3, 6 and 9 post tumor cell seeding, and the length and width of the
12 tumor spheroids were determined. The spheroid volume was calculated as: $V=1/2*L*W*W$ (L
13 and W being the length and width of the tumor spheroids, respectively). Five tumor spheroids
14 were calculated for each tested group.

15

16 ***In vivo* biodistribution**

17 U-87 MG cells were suspended in PBS (50 μ L, 2×10^6 cells), mixed with 25 μ L of Matrigel
18 (BASEMENT MEMBRANE MATRIX, BD Medical Technology, USA), and injected
19 subcutaneously into nude mice on the right flank. When the tumor volume reached 100 mm³
20 (usually within 10 days), PSP NPs or PPSP NPs containing Cy5-siRNA were intravenously (i.v.)
21 injected (1 mg siRNA/kg, 200 μ L). At 1 and 4 h post injection, animals were anesthetized with
22 3% isoflurane and imaged by a Maestro *In Vivo* Imaging System (PerkinElmer, MA, USA) using
23 green excitation filter (572-621 nm) with the exposure time of 100 ms. Mice were then

1 euthanized, and the tumors as well as major organs (heart, liver, spleen, lung, and kidney) were
2 harvested before being imaged using the Maestro *In Vivo* Imaging System as well. The tumor
3 tissues were further frozen in the OCT embedding medium (Sakura, CA, USA). Frozen sections
4 of 20- μm thickness were prepared with a cryotome Cryostat (CM 1900, Leica, Germany), and
5 were stained with Hoechst (300 nM) for 15min at room temperature. After washing with PBS for
6 twice, the frozen sections were mounted with the Prolong Gold[®] (Invitrogen) mounting medium
7 and observed under CLSM (Model 700, Zeiss, Germany).

8

9 ***In vivo* anti-cancer efficacy**

10 U-87 MG tumor-bearing mice were prepared as described above. When the tumor volume
11 reached 100 mm³, PSP NPs or PPSP NPs were i.v. injected at 1mg siRNA/kg every three days
12 for a total of three injections (6 mice in each group). PLL/siRNA NPs or saline served as controls.
13 The tumor size and body weight were monitored every 3 days within the observation period of
14 15 days. The tumor size was calculated as $V=1/2*L*W*W$ (L and W being the length and width
15 of the tumor, respectively).

16

17 ***In vivo* EGFR knockdown**

18 Tumors were harvested on day 15 post the first injection of NPs as described above (6 mice in
19 each group). RNA was isolated from tumors using the QIAGEN RNeasy Mini Kit, and the
20 EGFR mRNA level was determined by real-time PCR using the same method as mentioned
21 above. Results were denoted as the percentage of EGFR mRNA levels of the control mice that
22 did not receive NPs treatment.

1 The EGFR expression level was further explored by immunostaining. The tumors were fixed
2 with 4% PFA, frozen in OCT, and cryo-sectioned to obtained 20- μ m thick sections. They were
3 incubated with Anti-EGFR antibody (Santa Cruz Biotechnology, CA, USA) at 4°C overnight.
4 After washing with PBS for three times, the tumor sections were incubated with Alexa Fluor-555
5 labeled secondary antibody for another 2 h. Then, the sections were stained with Hoechst (300
6 nM) for 15 min at room temperature. After washing twice with PBS, the sections were mounted
7 with Prolong Gold[®] (Invitrogen) and observed by CLSM (Model 700, Zeiss, Germany).

8

9 **Results and discussion**

10 **Characterization, siRNA encapsulation, and stability of PSPP NPs**

11 PVBLG-8 possesses α -helical secondary structure, which is more rigid than other typical cationic
12 polymers that adopt flexible, random-coil structure. Although PVBLG-8 can condense plasmid
13 DNA to form stable NPs through electrostatic interaction,^{23, 28} it only forms loosely packed
14 complexes upon mixing with siRNA, presumably due to the rigid structure of both molecules
15 and the low molecular weight of siRNA that prohibit efficient complexation with PVBLG-8. The
16 resulting loosely packed complexes showed relatively large particle size of ~500 nm and high
17 polydispersity index (PDI) of 0.213, along with low siRNA encapsulation efficiency of <20% at
18 the PVBLG-8/siRNA weight ratio up to 20 (Fig. 1A). To address this issue, PLG, a random-
19 coiled polyanion, was incorporated as a stabilizer to facilitate the complexation between
20 positively charged PVBLG-8 and negatively charged siRNA and PLG, wherein PLG provided
21 sufficient molecular entanglement with PVBLG-8 to encapsulate the siRNA within the
22 polymeric network. PVBLG-8 was firstly complexed with PLG at different ratios as shown in
23 Table S3. The optimal PVBLG-8/PLG weight ratio of 10 was identified and used in further

1 studies, because of the relatively small particle size (~88 nm) and positive surface charge (~10
2 mV) of the PSP NPs at this ratio (Fig. S1A and B). In attempts to convert the surface charge of
3 NPs from positive to negative, additional PLG was coated onto the PSP NPs, yielding the
4 negatively charged PSPP NPs. As expected, zeta potential of the NPs decreased with increased
5 amount of coated PLG, and PSPP NPs with negative zeta potential were obtained at the PLG
6 (coating)/PVBLG-8 weight ratios ≥ 0.15 (Fig. S1B). Particle size slightly increased upon coating
7 with additional PLG (Fig. S1A). The optimal PLG (coating)/PVBLG-8 weight ratio of 0.15 was
8 identified, because of the smallest diameter and negative zeta potential of the PSPP NPs at such
9 ratio (PVBLG-8/siRNA/PLG (complexing)/PLG (coating) = 10/0.5/1/1.5, w/w/w/w). The siRNA
10 encapsulation efficiency was further evaluated using the EB exclusion assay and gel retardation
11 assay. In comparison to PVBLG-8/siRNA NPs that afforded siRNA encapsulation efficiency of
12 only ~10% at high weight ratio of 20, both PSP and PSPP NPs showed notably enhanced siRNA
13 encapsulation efficiencies of >80% at the PVBLG-8/siRNA weight ratio of 20 with fixed
14 PVBLG-8/PLG weight ratio (Fig. 1A). Similarly, the PSPP NPs were able to completely retard
15 the migration of siRNA upon agarose gel electrophoresis at the PVBLG-8/siRNA weight ratio \geq
16 2 (Fig. 1B), wherein PVBLG-8 alone could not retard the siRNA migration at the high PVBLG-
17 8/siRNA weight ratio up to 20 as reported in our previous research.²³ Because of the efficient
18 encapsulation of siRNA into the nanostructure, stability of siRNA against serum was greatly
19 enhanced as evidenced by the clear siRNA band after gel electrophoresis (Fig. 1C).
20 Comparatively, free siRNA was largely degraded after serum treatment for 2 h. After incubation
21 with serum, the particle size of the positively charged PSP NPs dramatically increased, while that
22 of the negatively charged PSPP NPs only slightly changed (Fig. 1D). It thus demonstrated that
23 surface coating of PSP NPs with additional PLG greatly enhanced the serum stability of the NPs

1 by shielding the positive surface charges, which would further benefit prolonged blood
2 circulation and tumor accumulation.⁴⁵

3

4 ***In vitro* cellular uptake of PSPP NPs**

5 We next studied the cellular uptake of PSPP NPs in U-87 MG glioblastoma cells at pH 6.5 (Fig.
6 2A). Compared with the positively charged PLL/siRNA NPs, cellular uptake level of the PSPP
7 NPs was 2.7 fold higher, presumably due to the high membrane activity of the exposed helical
8 PVBLG-8 from PSPP NPs at lowered pH in subcellular compartment that was capable of pore
9 formation to facilitate effective transmembrane delivery of gene cargoes.⁴⁶ To explore the
10 selectivity in terms of cellular internalization, HEK-293 cells (normal cell line) were incubated
11 with the PSPP NPs or PSP NPs at pH 7.4 and in the presence or absence of serum. Due to their
12 positively charged nature, PSP NPs showed appreciable cell uptake level in the absence of serum,
13 indicating lack of selectivity between normal and cancerous cells (Fig. S2). The cell uptake level
14 was dramatically diminished in the presence of serum, mainly because of the low stability of the
15 positively charged NPs in serum that led to particle aggregation/dissociation. In comparison,
16 PSPP NPs showed minimal cellular uptake level both in the presence and absence of serum at pH
17 7.4, because the surface coating of PLG shielded the cationic charges to prevent non-specific
18 cellular internalization in normal cells at neutral pH. Such findings therefore demonstrated that
19 PSPP NPs were capable of mediating selective and potent internalization into cancer cells due to
20 de-shielding of the PLG coating at acidic pH in the tumor extracellular compartment followed by
21 the helical PVBLG-8-mediated potent membrane penetration.

22 The successful delivery of siRNA into the cytoplasm of U-87 MG cells mediated by PSPP NPs
23 at pH 6.5 was also confirmed by CLSM (Fig. 2B). Extensive red fluorescence (Cy3-siRNA) was

1 noted in the cytoplasm, and it largely separated from the green fluorescence (Alexa Fluor 488-
2 labeled PLG), indicating that PSPP NPs efficiently delivered siRNA into U-87 MG cells and
3 siRNA could be released in the cytoplasm after cellular internalization.

4 To further study the endosomal escape of siRNA, a critical step toward effective gene
5 transfection, the endosome was stained with LysoTracker Green and its colocalization with Cy3-
6 siRNA was observed by CLSM. As shown in Fig. 2C, after 0.5-h incubation of cells with Cy3-
7 siRNA-containing PSPP NPs, Cy3-siRNA signal mainly co-localized with LysoTracker-stained
8 endosomes, suggesting that the PSPP NPs was internalized mainly through endocytosis.
9 Interestingly, after 2-h incubation, most of the Cy3-siRNA was found to spread out to the whole
10 cytoplasm, indicating the efficient endosomal escape of PSPP NPs mainly mediated by the
11 membrane disruption property of the helical PVBLG-8.

12

13 ***In vitro* EGFR silencing in U-87 MG cells**

14 The gene silencing efficiency of PSPP NPs against EGFR expression at pH 6.5 was evaluated in
15 U-87 MG cells by real-time PCR (Fig. 2D). The PSPP NPs led to 50% down-regulation of the
16 targeted EGFR mRNA level, which was comparable to knockdown efficiency of Lipofectamine
17 2000 (~60%). However, the PLL/siRNA NPs as a control only resulted in 23% down-regulation
18 of the EGFR mRNA level.

19

20 **Penetration of PSPP NPs in U-87 MG tumor spheroids**

21 The 3-D tumor spheroid was used to mimic the tumor tissues for the evaluation of tumor
22 penetration.⁴⁷ PSPP NPs prepared from Alexa Fluor 488-labeled PLG (green fluorescence) and
23 Cy3-siRNA (red fluorescence) were incubated with the tumor spheroids at pH 7.4 or 6.5, which

1 simulates the neutral condition during circulation and the acidic condition in the tumor
2 extracellular environment, respectively. Increased accumulation and deeper penetration of the
3 PSPP NPs in tumor spheroids were observed at pH 6.5 compared with those at pH 7.4 (Fig. 3A).
4 Cationic NPs normally exhibit higher tumor penetration capabilities than anionic NPs,⁴⁸ and thus
5 the above different tumor accumulation/penetration properties of PSPP NPs at different pH could
6 be attributed to the de-shielding of the PLG outer layer on the NPs surface that leads to the
7 exposure of the cationic PVBLG-8 to promote the tumor accumulation. PLL/siRNA NPs as a
8 control showed poor tumor penetration capability, and the Cy3-siRNA/Alexa Fluor 488-PLG
9 fluorescence was mainly localized on the periphery of the spheroids. Similar results were
10 obtained when the fluorescence distribution was further analyzed by Image J, revealing the deep
11 penetration of PSPP NPs into tumor spheroids compared to the peripheral distribution of
12 PLL/siRNA NPs (Fig. S3). To further explore the acid-triggered de-shielding of surface PLG
13 layers, the zeta potentials of PSPP NPs at different pH values from 7.4 to 5.5 were monitored in
14 collagen-coated tubes. As the pH decreased, the zeta potential of the NP increased and reversed
15 from negative to positive when pH reached 6.5 (Fig. 3B). It therefore verified the deprotonation
16 of the outer PLG layer and its depletion from the surface of PSPP NPs, which accordingly
17 allowed the exposure of PVBLG-8 because PLG was just loosely attached to the surface of PSP
18 NPs in a metastable state.

19

20 ***In vitro* gene silencing efficiency and anti-tumor efficacy of PSPP NPs in U-87 MG tumor** 21 **spheroids**

22 The extracellular environment of 3-D tumor spheroids was considered to be closer to that in the
23 *in vivo* settings. Therefore, the gene silencing efficiency of PSPP NPs against EGFR expression

1 in tumor spheroids was further determined by real-time PCR (Fig. 4A). The PSPP NPs led to 40%
2 down-regulation of the EGFR mRNA level in tumor spheroids at pH 6.5, while in comparison,
3 they showed negligible gene silencing at pH 7.4. On the other hand, the positively charged PSP
4 NPs showed comparable gene silencing effects at pH 7.4 and pH 6.5 in tumor spheroids. Such
5 discrepancy thus further substantiated that de-shielding of the PLG surface layer on PSPP NPs at
6 acidic pH could enable the selective delivery into tumor cells to mediate EGFR gene silencing.
7 PSPP NPs encapsulated with scrambled (sc) siRNA had no inhibitory effects on the EGFR
8 mRNA level at either pH 6.5 or pH 7.4.

9 Growth of the tumor spheroid after treatment with different NPs at pH 6.5 was further monitored
10 to evaluate the *in vitro* anti-cancer efficacy. The treatment began on the 3rd day of tumor
11 spheroid seeding (Day 3). After 3 days post-treatment (Day 6), size of the tumor spheroid treated
12 with PSPP NPs only increased by 6% compared with that of Day 3 (Fig. 4B), while the spheroids
13 treated with PLL/siRNA NPs or Lipofectamine 2000/siRNA NPs increased by ~50%. On day 9,
14 even obvious disparity was noted wherein spheroid volume after treatment with PSPP NPs was
15 only increased by 32%, while after treatment with PLL/siRNA NPs and Lipofectamine
16 2000/siRNA NPs, it was augmented by 84% and 102%, respectively. Such results further
17 indicated the potent efficiency of PSPP NPs in tumor growth inhibition over PLL/siRNA NPs
18 and Lipofectamine 2000/siRNA NPs.

19

20 ***In vivo* biodistribution and tumor accumulation of PSPP NPs**

21 The positively charged PSP NPs and negatively charged PSPP NPs were i.v. injected and the
22 whole animal fluorescence imaging was performed at 4 h post injection (Fig. 5A). Animals
23 receiving PSPP NPs showed notably stronger fluorescence signals in the tumor regions than

1 those treated with PSP NPs. Similar results were observed when the tumor tissues were
2 harvested and imaged, wherein the fluorescence intensity in PSPP NPs-treated tumors was
3 comparable to that in PSPP NPs-treated liver tissues while notably higher than that in PSP NPs-
4 treated tumors (Fig. 5B-E). Such disparity was mainly because the negatively charged PSPP NPs
5 could prevent the adsorption of serum proteins and thus prolong the blood circulation time and
6 passive cancer targeting. CLSM observation of tumor sections also showed higher distribution
7 level of Cy3-siRNA in PSPP NPs-treated tumors than in PSP NP-treated tumors (Fig. 5E), and
8 the signals were mainly concentrated in the intracellular areas, indicating that PSPP NPs could
9 be distributed to the tumor in a more effective way, and PVBLG-8 could mediate effective cell-
10 penetration and endosomal escape after entering the tumor cells.

11

12 ***In vivo* anti-tumor efficacy**

13 Nude mice bearing U-87 MG xenograft tumors were i.v. injected with different NPs as well as
14 saline. The treatment began when the tumor volume reached 100 mm³ as the EPR effect was
15 considered to be prevalent at this stage.^{49,50} The body weights did not change significantly after
16 administration of different NPs, indicating their unappreciable toxicity (Fig. S4). Tumor growth
17 was notably inhibited after treatment with PSPP NPs containing EGFR siRNA, and it
18 significantly outperformed the PLL/siRNA NPs and PSP NPs in terms of the anti-tumor efficacy
19 (Fig. 6A). Consistently, PSPP NPs mediated significantly higher EGFR silencing efficiency than
20 PLL/siRNA NPs and PSP NPs in tumor tissues, as evidenced by both real-time PCR (Fig. 6B)
21 and EGFR immunostaining (Fig. 6C). The quantitative immunostaining analysis was
22 shown in Fig. S5. Such results accorded well with the *in vitro* results to substantiate the

1 collective contribution of PLG-promoted tumor accumulation and PVBLG-8-mediated
2 membrane penetration toward efficient EGFR siRNA delivery and anti-tumor treatment.

3

4 **Conclusions**

5 In summary, metastable NPs capable of tumor targeting, tumor penetration, and selective tumor
6 cell internalization were developed based on membrane penetrating, helical polypeptide
7 PVBLG-8 and anionic PLG, for the efficient encapsulation and delivery of EGFR siRNA. The
8 rigid, linear structure of PVBLG-8 suffered from poor siRNA condensation capability, and PLG
9 with linear and flexible chains was incorporated as a stabilizer to enhance the molecular
10 entanglement with PVBLG-8 to remarkably strength the siRNA encapsulation. The obtained PSP
11 NPs with positive surface charges were further coated with PLG to reverse the surface charge
12 from positive to negative, and thus the obtained PSPP NPs featured desired serum stability
13 during circulation to enhance tumor accumulation via the EPR effect. After accumulation of the
14 PSPP NPs in the tumor tissues, the acidic extracellular condition (pH 6.5) triggered de-shielding
15 of the PLG coating to expose the cationic, membrane-penetrating PVBLG-8, thus facilitating
16 tumor penetration, cancer cell uptake, and endosomal escape of the NPs. Unlike the tumor cell
17 endocytosis enhanced by ligand-receptor interaction, PVBLG-8-mediated intracellular delivery
18 showed a receptor-independent pathway which was more efficient and universal that could also
19 be applied in other tumor types. As a result, the PSPP NPs efficiently silenced the EGFR
20 expression in U-87 MG tumor spheroids in vitro and tumor tissues in vivo, and notably inhibited
21 the growth of tumor spheroids in vitro and xenograft tumors in vivo, outperforming the PSP NPs
22 and commercial reagents such as Lipofectamine 2000 and PLL. Considering that acidic
23 extracellular condition is a common microenvironment characteristic shared by most tumors, the

1 PSPP NPs developed in this study can be further explored as a universal siRNA delivery
2 nanoplatform for targeted and efficient cancer gene therapy.

3

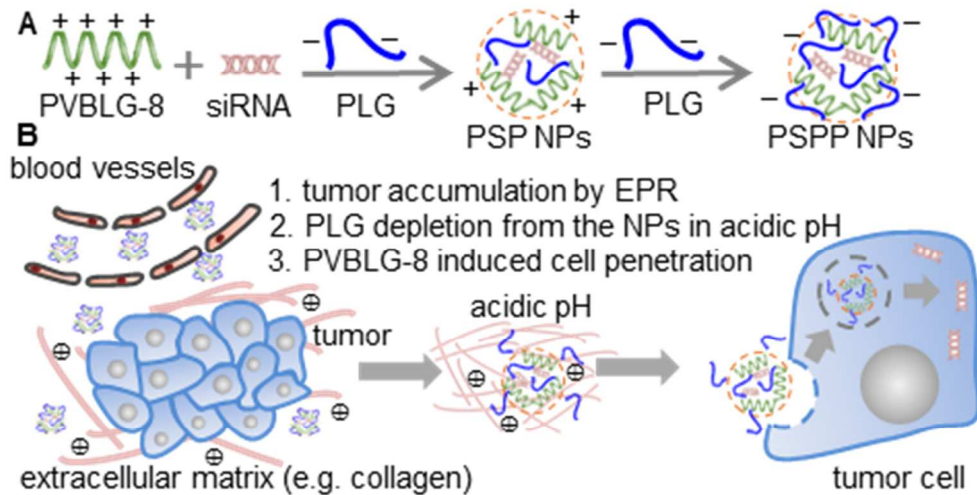
4 **Conflicts of interest**

5 There are no conflicts to declare.

6

7 **Acknowledgements**

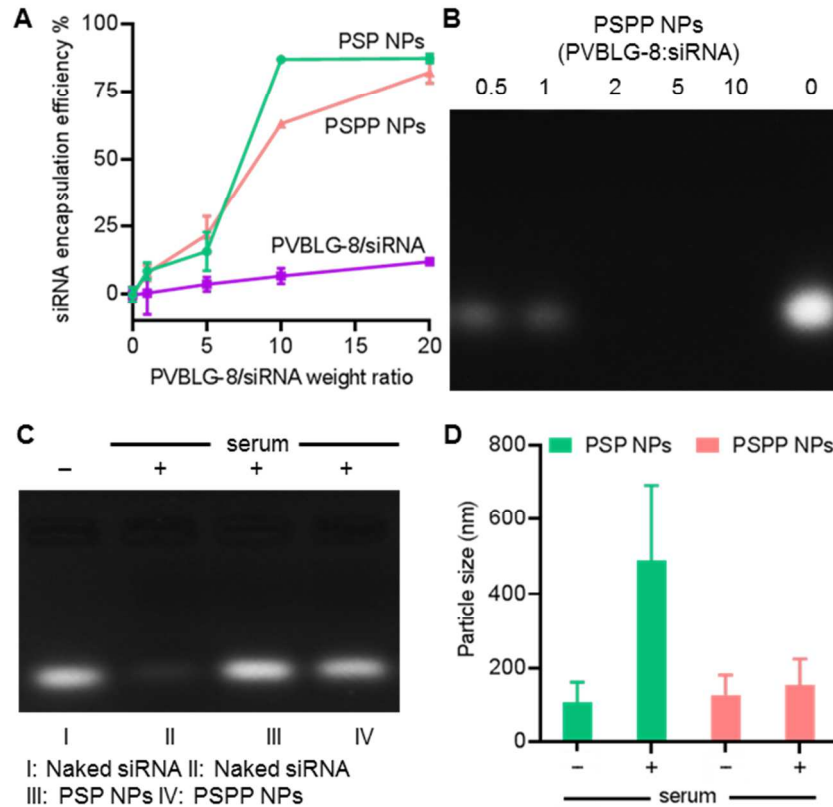
8 J.C. acknowledges support from NSF (CHE 1709820) for materials development and the NIH
9 (1R01CA207584) for biological evaluations. L.Y. acknowledges the financial support from the
10 National Natural Science Foundation of China (51573123 and 51722305), the Ministry of
11 Science and Technology of China (2016YFA0201200), and Priority Academic Program
12 Development of Jiangsu Higher Education Institutions.



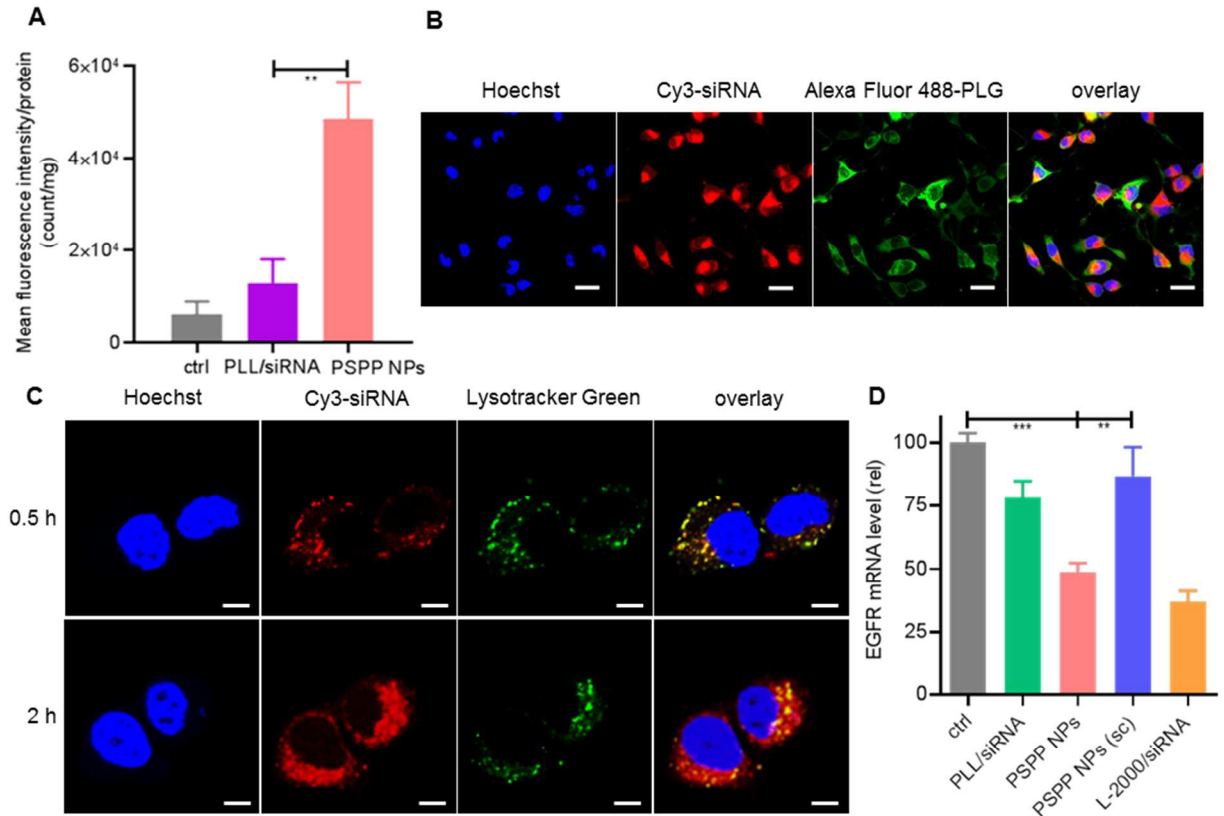
1

2 **Scheme 1.** Tumor-targeted siRNA delivery mediated by metastable NPs based on cell
 3 penetrating α -helical polypeptide, PVBLG-8. (A) PLG is incorporated during the formation of
 4 PVBLG-8/siRNA complexes to facilitate and stabilize the formation of positively charged PSP
 5 NPs. They were further coated with additional PLG to yield negatively charged PPSP NPs with
 6 increased serum stability and prolonged blood circulation. (B) After accumulation of the PPSP
 7 NPs in the tumor tissues through the EPR effect, the acidic extracellular pH triggers detachment
 8 of the PLG outer shell from the NPs surface, thus exposing the membrane-active PVBLG-8 to
 9 induce efficient cellular internalization of NPs.

10

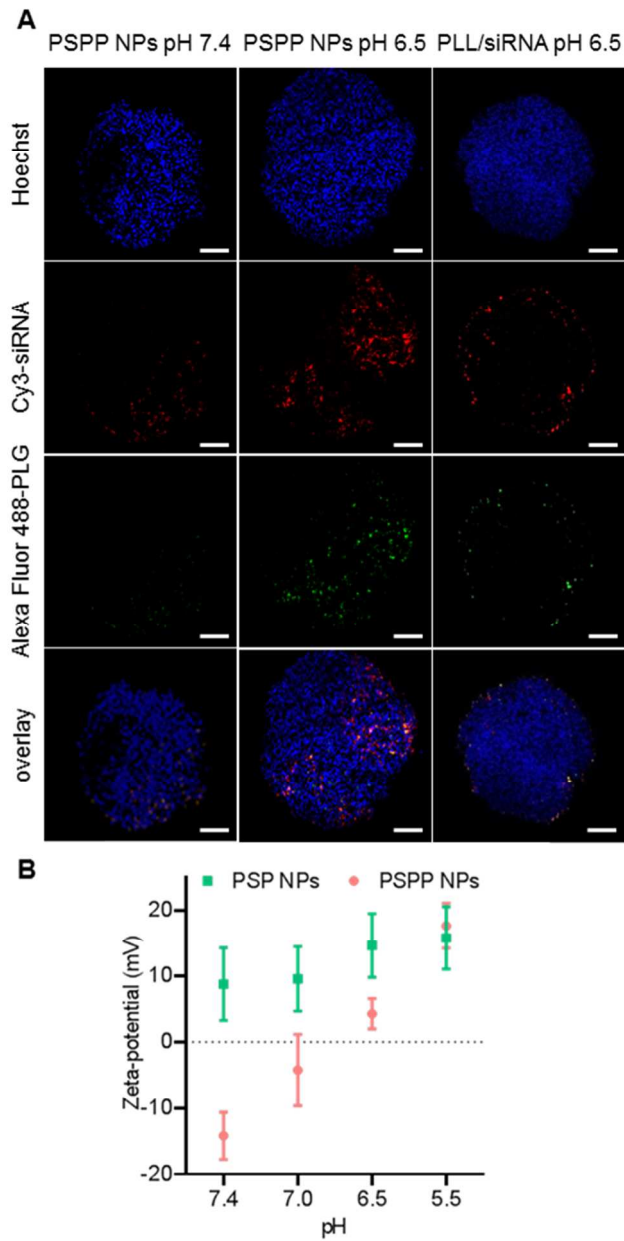


1
 2 **Fig. 1** Characterization of NPs. (A) siRNA encapsulation efficiencies in PS, PSP, and PPSP NPs
 3 as determined by the EB exclusive assay. (B) Gel retardation assay showing siRNA migration in
 4 4% agarose gel. PSPP NPs with various PVBLG-8/siRNA weight ratios were utilized (PVBLG-
 5 8/PLG = 10:1.5, w/w). (C) Gel retardation assay for stability of naked siRNA or siRNA loaded
 6 in NPs following treatment with mouse serum for 2 h. (D) Size alteration of PSP and PSPP NPs
 7 upon incubation with 10% mouse serum for 2 h.

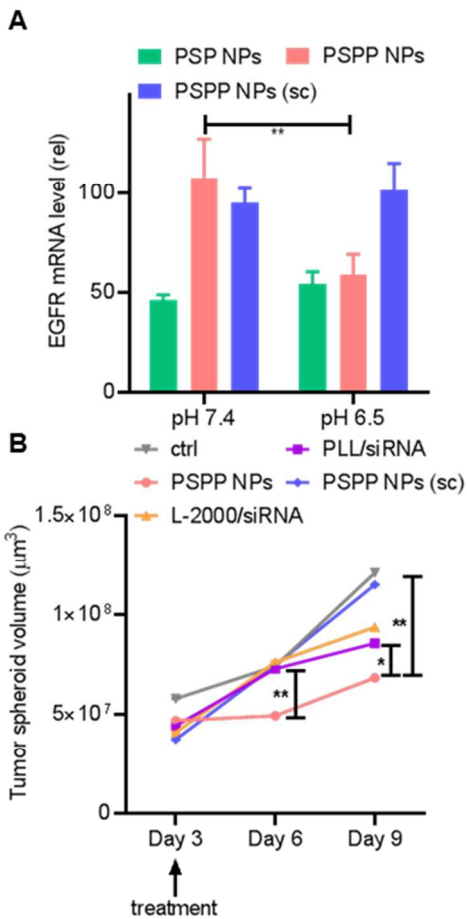


1
 2 **Fig. 2** *In vitro* cell uptake of NPs and EGFR knockdown in U-87 MG cells. (A) Cellular uptake
 3 level of Cy3-siRNA-loaded NPs at pH 6.5 (n = 4, * p < 0.05; ** p < 0.005; *** p < 0.001). (B)
 4 CLSM images of U-87 MG cells after treatment with PSPP NPs containing Cy3-siRNA (red)
 5 and Alexa Fluor 488-PLG (green) for 4 h at pH 6.5. Cell nuclei were stained with Hoechst (blue).
 6 Bar represents 5 μ m. (C) CLSM images U-87 MG cells following treatment with PSPP NPs
 7 loaded with Cy3-siRNA (red) at pH 6.5 for 0.5 or 2 h. Cell nuclei were stained with Hoechst
 8 (blue), and endo-lysosomes were stained with Lysotracker Green (green). Bar represents 5 μ m.
 9 (D) Relative EGFR mRNA level in U-87 MG cells after treatment with various NPs at pH 6.5 (n
 10 = 4, , * p < 0.05; ** p < 0.005; *** p < 0.001).

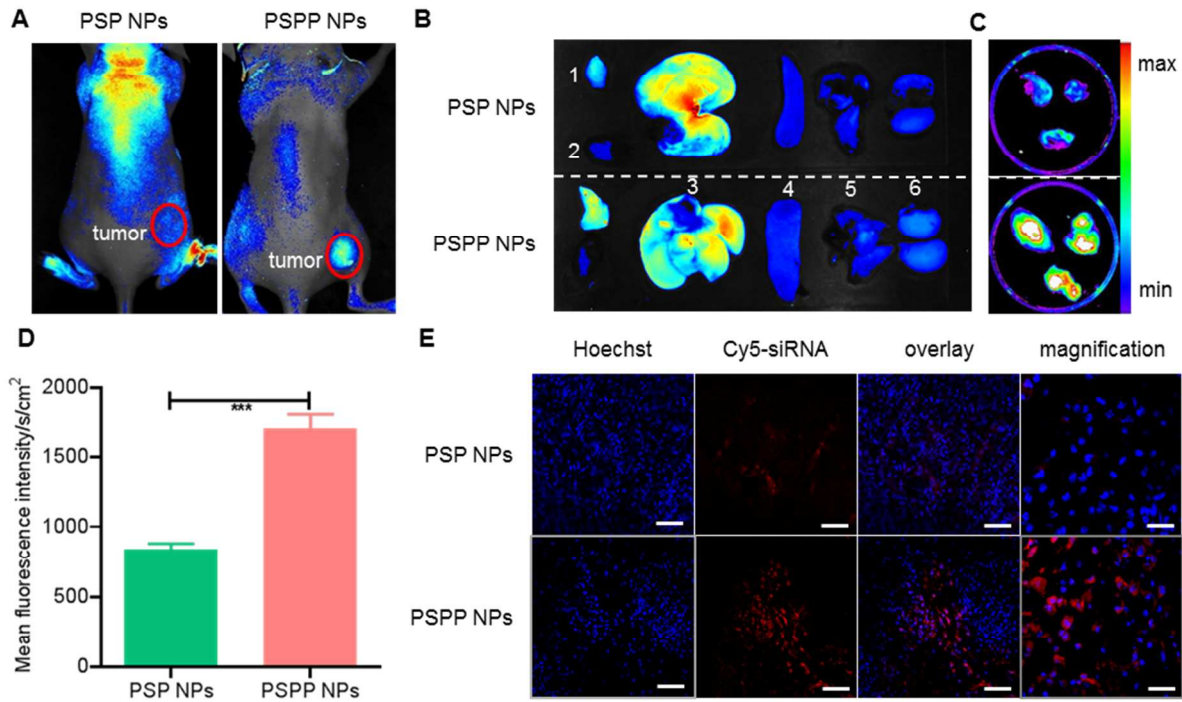
11



1
 2 **Fig. 3** (A) Acid-mediated de-shielding of PLG surface layers on PSPP NPs promotes tumor
 3 penetration of PPSP NPs. (A) CLSM images of U-87 MG tumor spheroids following treatment
 4 with Cy3-siRNA-containing PPSP NPs at pH 7.4 or 6.5 for 4 h. PLL/siRNA NPs were
 5 incorporated as a control. Scale bar represents 250 μm . (B) Zeta potentials of PSP NPs and PPSP
 6 NPs at different pH.

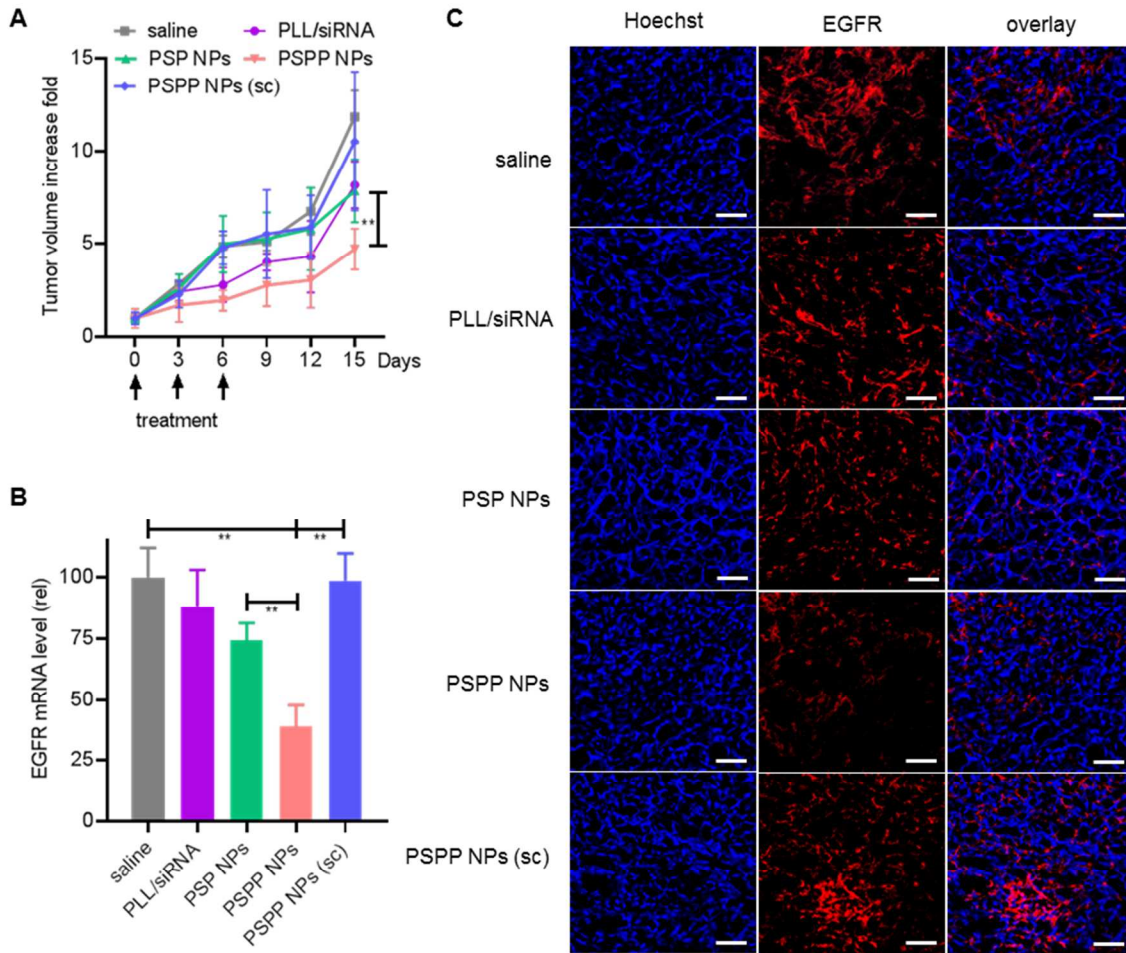


1
 2 **Fig. 4** EGFR silencing and anti-tumor efficacy of PSPP NPs in U-87 MG tumor spheroids. (A)
 3 EGFR mRNA levels in tumor spheroids after treatment with various NPs at pH 7.4 or 6.5 (n = 3,
 4 * p < 0.05; ** p < 0.01; *** p < 0.001). (B) Volume changes of tumor spheroids within 6 days
 5 following treatment with various NPs at pH 6.5 (n = 5, * p < 0.05; ** p < 0.005; *** p < 0.001).
 6



1
 2 **Fig. 5** Biodistribution of Cy5-siRNA-containing PSP or PSPP NPs in U-87 MG tumor-bearing
 3 mice at 4 h post i.v. injection (1 mg siRNA/kg). (A) Fluorescence imaging of whole animals. (B)
 4 Representative *ex vivo* imaging of tumors and major organs. 1. tumor, 2. heart, 3. liver, 4. spleen,
 5 5. lung, and 6. kidney. (C) *Ex vivo* imaging of tumors harvested from mice administered with
 6 PSP NPs (top) and PSPP NPs (bottom) (n = 3). (D) Calculated fluorescence intensities of Cy5-
 7 siRNA in *ex vivo* tumors in (C) (n = 3, * p < 0.05; ** p < 0.005; *** p < 0.001). (E) CLSM
 8 images of tumor sections. Nuclei were stained with Hoechst. Scale bars represent 10 µm in
 9 column 1-3 and 2 µm in column 4.

10



1
 2 **Fig. 6** EGFR knockdown efficiency and anti-tumor efficacy of i.v. injected NPs (1mg siRNA/kg)
 3 in U-87 MG xenograft tumor-bearing mice. (A) Tumor volume changes over the observation
 4 period of 15 days (n = 6, * p < 0.05; ** p < 0.005; *** p < 0.001). (B) Relative EGFR mRNA
 5 levels in tumors on Day 15 post the first NPs injection (n = 6, * p < 0.05; ** p < 0.005; *** p <
 6 0.001). (C) EGFR immunostaining of tumor sections harvested on Day 15 post the first NPs
 7 injection. Cell nuclei were stained with Hoechst. Scale bar represents 10 μ m.

8

9

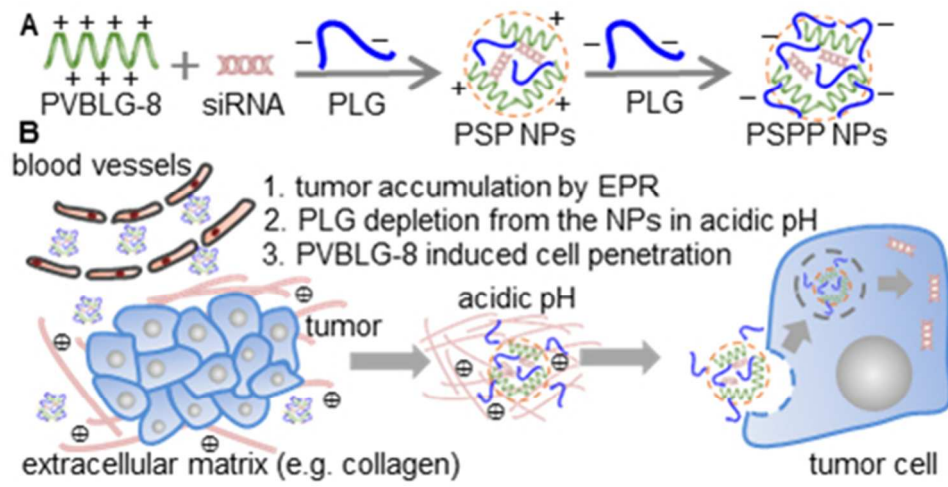
10

11

1 **References**

- 2 1. R. Kanasty, J. R. Dorkin, A. Vegas and D. Anderson, *Nat. Mater.*, 2013, **12**, 967-977.
- 3 2. N. P. Gabrielson, H. Lu, L. Yin, D. Li, F. Wang and J. Cheng, *Angew Chem. Int. Ed.*
- 4 *Engl.*, 2012, **51**, 1143-1147.
- 5 3. H. M. Ali, G. Urbinati, M. Raouane and L. Massaad-Massade, *Expert Rev. Clin.*
- 6 *Pharmacol.*, 2012, **5**, 403-412.
- 7 4. A. de Fougerolles, H. P. Vornlocher, J. Maraganore and J. Lieberman, *Nat. Rev. Drug*
- 8 *Discov.*, 2007, **6**, 443-453.
- 9 5. Y. Li, H. Bai, H. Wang, Y. Shen, G. Tang and Y. Ping, *Nanoscale*, 2017, **10**, 203-214.
- 10 6. C. K. Chen, W. C. Law, R. Aalinkeel, Y. Yu, B. Nair, J. Wu, S. Mahajan, J. L. Reynolds,
- 11 Y. Li, C. K. Lai, E. S. Tzanakakis, S. A. Schwartz, P. N. Prasad and C. Cheng, *Nanoscale*,
- 12 2014, **6**, 1567-1572.
- 13 7. S. Bhunia, V. Radha and A. Chaudhuri, *Nanoscale*, 2017, **9**, 1201-1212.
- 14 8. N. K. Ryoo, J. Lee, H. Lee, H. K. Hong, H. Kim, J. B. Lee, S. J. Woo, K. H. Park and H.
- 15 Kim, *Nanoscale*, 2017, **9**, 15461-15469.
- 16 9. A. Daka and D. Peer, *Adv. Drug Deliv. Rev.*, 2012, **64**, 1508-1521.
- 17 10. S. Quasthoff and H. P. Hartung, *J. Neurol.*, 2002, **249**, 9-17.
- 18 11. T. A. Ahles, A. J. Saykin, C. T. Furstenberg, B. Cole, L. A. Mott, K. Skalla, M. B.
- 19 Whedon, S. Bivens, T. Mitchell, E. R. Greenberg and P. M. Silberfarb, *J. Clin. Oncol.*,
- 20 2002, **20**, 485-493.
- 21 12. D. H. Kim and J. J. Rossi, *Nat. Rev. Genet.*, 2007, **8**, 173-184.
- 22 13. B. Ozpolat, A. K. Sood and G. Lopez-Berestein, *Adv. Drug Deliv. Rev.*, 2014, **66**, 110-
- 23 116.
- 24 14. J. C. Burnett, J. J. Rossi and K. Tiemann, *Biotechnol. J.*, 2011, **6**, 1130-1146.
- 25 15. S. Gao, H. Tian, Z. Xing, D. Zhang, Y. Guo, Z. Guo, X. Zhu and X. Chen, *J. Control.*
- 26 *Release*, 2016, **243**, 357-369.
- 27 16. R. Molinaro, J. Wolfram, C. Federico, F. Cilurzo, L. Di Marzio, C. A. Ventura, M.
- 28 Carafa, C. Celia and M. Fresta, *Expert Opin. Drug Deliv.*, 2013, **10**, 1653-1668.
- 29 17. J. Beloor, C. S. Choi, H. Y. Nam, M. Park, S. H. Kim, A. Jackson, K. Y. Lee, S. W. Kim,
- 30 P. Kumar and S. K. Lee, *Biomaterials*, 2012, **33**, 1640-1650.
- 31 18. C. He, Y. Hu, L. Yin, C. Tang and C. Yin, *Biomaterials*, 2010, **31**, 3657-3666.
- 32 19. J. Liu, S. Iqbal, X. J. Du, Y. Yuan, X. Yang, H. J. Li and J. Wang, *Biomater. Sci.*, 2017,
- 33 DOI: 10.1039/c7bm01025g.
- 34 20. R. A. Petros and J. M. DeSimone, *Nat. Rev. Drug Discov.*, 2010, **9**, 615-627.
- 35 21. H. Hatakeyama, H. Akita and H. Harashima, *Adv. Drug Deliv. Rev.*, 2011, **63**, 152-160.
- 36 22. H. Hatakeyama, H. Akita, E. Ito, Y. Hayashi, M. Oishi, Y. Nagasaki, R. Danev, K.
- 37 Nagayama, N. Kaji, H. Kikuchi, Y. Baba and H. Harashima, *Biomaterials*, 2011, **32**,
- 38 4306-4316.
- 39 23. N. P. Gabrielson, H. Lu, L. Yin, K. H. Kim and J. Cheng, *Mol. Ther.*, 2012, **20**, 1599-
- 40 1609.
- 41 24. L. Yin, Z. Song, K. H. Kim, N. Zheng, N. P. Gabrielson and J. Cheng, *Adv. Mater.*, 2013,
- 42 **25**, 3063-3070.
- 43 25. L. Yin, Z. Song, K. H. Kim, N. Zheng, H. Tang, H. Lu, N. Gabrielson and J. Cheng,
- 44 *Biomaterials*, 2013, **34**, 2340-2349.

- 1 26. L. Yin, Z. Song, Q. Qu, K. H. Kim, N. Zheng, C. Yao, I. Chaudhury, H. Tang, N. P.
2 Gabrielson, F. M. Uckun and J. Cheng, *Angew Chem. Int. Ed. Engl.*, 2013, **52**, 5757-5761.
- 3 27. L. Yin, H. Tang, K. H. Kim, N. Zheng, Z. Song, N. P. Gabrielson, H. Lu and J. Cheng,
4 *Angew. Chem. Int. Ed. Engl.*, 2013, **52**, 9182-9186.
- 5 28. N. Zheng, L. Yin, Z. Song, L. Ma, H. Tang, N. P. Gabrielson, H. Lu and J. Cheng,
6 *Biomaterials*, 2014, **35**, 1302-1314.
- 7 29. R. Gref, A. Domb, P. Quellec, T. Blunk, R. H. Muller, J. M. Verbavatz and R. Langer,
8 *Adv. Drug Deliv. Rev.*, 1995, **16**, 215-233.
- 9 30. M. Li, W. Song, Z. Tang, S. Lv, L. Lin, H. Sun, Q. Li, Y. Yang, H. Hong and X. Chen,
10 *ACS Appl. Mater. Interfaces*, 2013, **5**, 1781-1792.
- 11 31. W. Song, M. Li, Z. Tang, Q. Li, Y. Yang, H. Liu, T. Duan, H. Hong and X. Chen,
12 *Macromol. Biosci.*, 2012, **12**, 1514-1523.
- 13 32. T. Akagi, H. Kim and M. Akashi, *J. Biomater. Sci. Polym. Ed.*, 2010, **21**, 315-328.
- 14 33. K. Zhang, X. Zhu, F. Jia, E. Auyeung and C. A. Mirkin, *J. Am. Chem. Soc.*, 2013, **135**,
15 14102-14105.
- 16 34. L. Miao, C. M. Lin and L. Huang, *J. Control. Release*, 2015, **219**, 192-204.
- 17 35. E. A. Vasievich and L. Huang, *Mol. Pharm.*, 2011, **8**, 635-641.
- 18 36. X. Guan, Z. Guo, T. Wang, L. Lin, J. Chen, H. Tian and X. Chen, *Biomacromolecules*,
19 2017, **18**, 1342-1349.
- 20 37. Z. Guo, J. Chen, L. Lin, X. Guan, P. Sun, M. Chen, H. Tian and X. Chen, *ACS Appl.*
21 *Mater. Interfaces*, 2017, **9**, 15297-15306.
- 22 38. Y. Yu, C. K. Chen, W. C. Law, E. Weinheimer, S. Sengupta, P. N. Prasad and C. Cheng,
23 *Biomacromolecules*, 2014, **15**, 524-532.
- 24 39. X. Chen, L. Liu and C. Jiang, *Acta Pharm. Sin. B*, 2016, **6**, 261-267.
- 25 40. M. Dimde, F. Neumann, F. Reisbeck, S. Ehrmann, J. L. Cuellar-Camacho, D. Steinhilber,
26 N. Ma and R. Haag, *Biomater. Sci.*, 2017, **5**, 2328-2336.
- 27 41. X. He, J. Li, S. An and C. Jiang, *Ther. Deliv.*, 2013, **4**, 1499-1510.
- 28 42. P. Xu, E. A. Van Kirk, Y. Zhan, W. J. Murdoch, M. Radosz and Y. Shen, *Angew Chem.*
29 *Int. Ed. Engl.*, 2007, **46**, 4999-5002.
- 30 43. B. R. Voldborg, L. Damstrup, M. Spang-Thomsen and H. S. Poulsen, *Ann. Oncol.*, 1997,
31 **8**, 1197-1206.
- 32 44. J. Du, W. L. Lu, X. Ying, Y. Liu, P. Du, W. Tian, Y. Men, J. Guo, Y. Zhang, R. J. Li, J.
33 Zhou, J. N. Lou, J. C. Wang, X. Zhang and Q. Zhang, *Mol. Pharm.*, 2009, **6**, 905-917.
- 34 45. X. Guan, Z. Guo, L. Lin, J. Chen, H. Tian and X. Chen, *Nano Lett.*, 2016, **16**, 6823-6831.
- 35 46. R. Zhang, Z. Song, L. Yin, N. Zheng, H. Tang, H. Lu, N. P. Gabrielson, Y. Lin, K. Kim
36 and J. Cheng, *Wiley Interdiscip Rev. Nanomed. Nanobiotechnol.*, 2015, **7**, 98-110.
- 37 47. J. Bugno, H. J. Hsu, R. M. Pearson, H. Noh and S. Hong, *Mol. Pharm.*, 2016, **13**, 2155-
38 2163.
- 39 48. T. Jiang, Z. Zhang, Y. Zhang, H. Lv, J. Zhou, C. Li, L. Hou and Q. Zhang, *Biomaterials*,
40 2012, **33**, 9246-9258.
- 41 49. S. Guo, L. Lv, Y. Shen, Z. Hu, Q. He and X. Chen, *Sci. Rep.*, 2016, **6**, 21459.
- 42 50. Y. Sakurai, T. Hada, S. Yamamoto, A. Kato, W. Mizumura and H. Harashima, *Mol.*
43 *Ther.*, 2016, **24**, 2090-2099.



83x43mm (150 x 150 DPI)